Indian Journal of Engineering & Materials Sciences
Vol. 28, June 2021, pp. 300-310

Effect of process parameters on tensile strength and surface quality of PLA-ABS part

Mohanraj Ramasamy*, Elangovan Sooriya Moorthy, Arunkarthik Balasubramanian, Pratheesh Kumar Selva Kumaran, Maaz Baig Nayaz Baig, Shriram Alagappan & Muneeskumar Moorthy

Department of Production Engineering, PSG College of Technology, Coimbatore 641 004, India

Received: 12 September 2020; Accepted: 12 April 2021

Fused Deposition Modeling (FDM) is an additive manufacturing technology to fabricate three-dimensional prototypes with complex geometries. The ultimate tensile strength and surface finish of the parts produced by FDM process are strongly related to the fabrication process parameters. So it is necessary to identify the optimal process parameters to improve the ultimate tensile strength and surface finish of the part. FDM process has been influenced by many process parameters and the process parameters such as raster angle, infill pattern and build orientation have been considered in this study to determine their influence on the response parameters such as ultimate tensile strength and surface roughness of Polylactic Acid (PLA)-Acrylonitrile Butadiene Styrene (ABS) blend. In this work, an experimental study has been validated using the response surface methodology and influence of the process parameters on response parameters has been analyzed using analysis of variance (ANOVA) method. Scanning Electron Microscope (SEM) images have been used to study the microstructure of the specimen at the fracture interface. The result has shown that infill pattern is the significant factor affecting the ultimate tensile strength. Surface roughness of the specimen has been found influenced by the build orientation followed by the infill pattern and raster angle.

Keywords: Fused deposition modeling (FDM), Response surface methodology, Ultimate tensile strength, Surface roughness, Scanning electron microscope (SEM)

1 Introduction

Additive manufacturing is an advanced manufacturing technology to fabricate three-dimensional (3D) objects by adding materials in a layer by layer approach based on part design. 3D printing technology has been developed to manufacture the complex structures with less lead time to satisfy the market requirements[1]. Aircraft, Automobile and bio-medical industries use 3D printing technology to manufacture functional and physical prototype for real time and research applications[2]. Additive manufacturing process are classified based on the form of materials used to develop 3D parts and manufacturing technologies such as selective laser sintering, fused deposition modeling, stereo-lithography apparatus, inkjet modeling, 3D printing and direct metal deposition.

Fused Deposition Modeling (FDM) is one of the commonly used techniques in additive manufacturing process to produce complex 3D geometrical profiles using thermoplastics. Thermoplastic material in the form of solid wire is melted into liquid state upon heating and deposited on a platform through a nozzle as shown in Fig. 1. The nozzle traces the cross section pattern of part geometry to produce 3D part with the thermoplastic material where it solidifies before the deposition of next layer[3]. The bonding between each layer takes place by means of diffusion welding principle. The most commonly used thermoplastic printable materials for the FDM process are Acrylonitrile Butadiene Styrene (ABS), Polylactic Acid (PLA) and Polycarbonate (PC). Fused Deposition Modeling process produce parts with high accuracy, improved quality with low manufacturing cost[4,5].

FDM process starts with the design of Computer Aided Design (CAD) model of the part and its conversion into a STL file format. The generated STL file has been imported into the in-build software of the FDM machine which slices the CAD model into thin layers and assigns machine attributes. The sliced layer provides the two dimensional cross-section data of the designed model and G-code has been generated based on the data to control the FDM machine[6].

*Corresponding author (E-mail: mohanraj839@gmail.com)

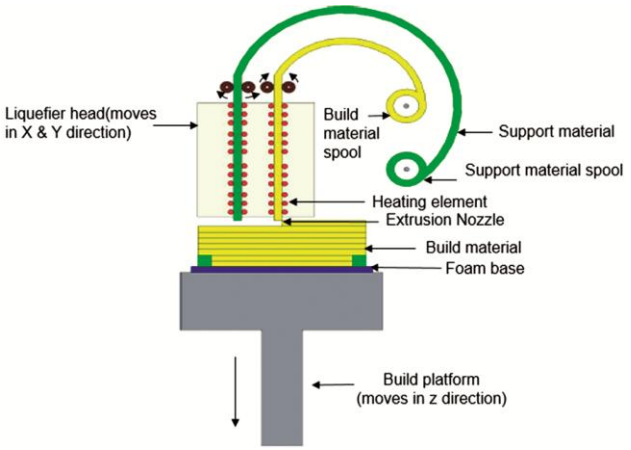

Fig. 1 — Schematic representation of FDM system.

Mohamed *et al.*[7] has studied the influence of FDM process parameters on surface roughness, mechanical properties, dimensional accuracy, build time, material behavior and dynamic mechanical properties of PC-ABS material by using I-optimal design response surface methodology approach. The study concludes that dynamic mechanical properties are maximum influenced by the raster to raster air gap, the number of outlines, slice thickness, road width and build orientation. It has been found that raster angle has minimum influence on these properties. Garg *et al.*[8] have investigated the failure of parts produced at selected range of raster angles under flexural and tensile loading of ABS material. Raster angles of 0°, 30°, 60° and 90° are considered for surface roughness, tensile and flexural testing and concluded that raster angle of 0° have high tensile strength of 35 MPa and high flexural strength of 52 MPa with better surface finish. Liu *et al.*[9] have used Taguchi method to investigate the influence of FDM process parameters such as deposition orientation, deposition style, raster width, layer thickness and raster gap on tensile strength, flexural strength, and impact strength of PLA material. The result shows that deposition orientation followed by layer thickness and deposition styles are the most significant factor which affects the mechanical properties.

Park *et al.*[10] have studied the thermal distribution of thermoelastic stress analysis on themechanical strength of the PLA material by using the passive infrared thermography technique. The result shows that raster angle and annealing are important influencing factors on determining thermoelastic effect because of their relation to delamination and crystallinity which increases the thermoelastic effect. Samykano *et al.*[11] have applied response surface methodology to study the influence of FDM process parameters such as layer height, infill density and raster angle on mechanical properties of ABS material. The result shows that infill percentage of 80%, layer thickness of 0.5 mm, and raster angle of 65° are the optimal process parameters. The ultimate tensile strength of 31.57 MPa, elastic modulus of 774.50 MPa and yield strength of 19.95 MPa are maximum value achieved from the experimental investigations.

Srivastava *et al.*[12] have studied the effect of FDM process parameters such as contour width, raster angle, spatial orientation and air gap on build time and material volume of ABS material response surface methodology and fuzzy logic technique. It has been found that the air gap of 0.0254 mm, orientation angle of 30° and raster angle of 0° obtained minimal values of build time of 1.083 hours and model material volume of 7.264 cm^3. Zaman *et al.*[13] have investigated the impact of layer thickness, infill pattern, infill percentage and shells on compressive strength of build parts on PLA material using Taguchi design of experiments. The study concludes that the infill percentage is the most dominating parameter in influencing the compressive strength. The result shows that layer thickness of 0.2 mm, 4 numbers of shells, diamond infill pattern, infill density of 70% are the optimum combination to improve the compressive strength.

Kuo *et al.*[14] have investigated to minimize the warpage of ABS prototypes by using Taguchi design of experiments. It has been found that the warpage can be minimized by using print speed of 60 mm/s, temperature of nozzle, bed and chamber at 230°C, 93°C and 43°C respectively. The bed temperature and chamber temperature were found as the dominant factors influencing the warpage of ABS prototypes. Kelkar *et al.*[15] have proposed a methodology to measure surface roughness of the part manufactured using FDM process. Conventional stylus instrument and light sectioning vision system are used to measure surface roughness. Light sectioning method, as it is non-contact and reliable method. It has been found that light sectioning method is more efficient for surface roughness measurement of FDM parts which shows better accuracy in results compared to conventional stylus measurement technique.

Jo *et al.*[16] have considered three post-processing methods such as resin infiltration, dipping method and

fumigation method to enhance surface roughness, mechanical strength and tightness of the FDM part. It has been found that resin infiltration provides better surface finish, strength, shrinkage and tightness by infiltrating the resins in porous structure of the part. Jin *et al.*[17] have developed a theoretical model to investigate the surface topography between adjacent layers and tensile properties of PLA material considering chemical finishing. The experimental results have been compared with the theoretical computed values and found that the deviations are due to measurement error. After chemical finishing, thin transparent film formed on the surface of the part improved the toughness properties and elongations at break was improved by 50%.

Ang *et al.*[18] have investigated the effects of air gap, raster width, build profile, build orientation and build layers on mechanical properties and porosity relationships in fabricated porous structures on ABS material by using the two level fractional factorial design. It has been found that the raster width and air gap affects the mechanical properties and porosity of the ABS scaffold structures. Dawoud *et al.*[19] have investigated the processing method effect on the mechanical property of ABS material using fused deposition modeling and injection moulding process. The result shows that an optimal selection of FDM parameters will improve the mechanical property of the part compared to injection moulding in static and dynamic loading conditions. Ning *et al.*[20] have studied the tensile and flexural properties of carbon fiber reinforced thermoplastic composites of ABS material using FDM process. ABS pellets and carbon fibers with different percentages such as 3%, 5%, 7.5%, 10% and 15% have been used to fabricate specimens. Fracture interface after tensile and flexural testing of specimens have been analyzed using scanning electron microscope to identify the optimum carbon fiber percentage and length of carbon fiber to improve the mechanical properties. It has been found that the 5% of carbon content and carbon length of 150 μm yields the highest tensile and flexural strength.

Most of the researchers have investigated the influence of FDM process parameters on mechanical properties of ABS and PC materials. The parts manufactured by FDM process limits the application due to poor surface characteristics and lack of mechanical properties. Due to the improper selection of process parameters as shown in Fig. 2, FDM processed parts posses poor surface quality and mechanical properties[9]. The PLA-ABS material can be used for wide variety of application but the characteristics of material on FDM process needs to be understood to determine the suitability of material. The surface finish and tensile property of the PLA-ABS material is an important characteristic which needs to be identified. The part with high engineering characteristics has been attained through proper selection of essential process parameters[21]. The influence of FDM process parameters on surface roughness and tensile strength of PLA-ABS material need to be indentified for industrial applications.

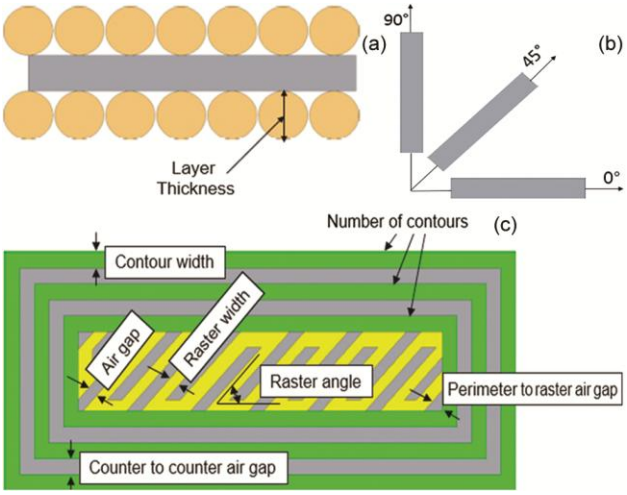

Fig. 2 — FDM process conditions (a) layer thickness, (b) build orientation and (c) tool path.

The aim of the work is to study the influence of FDM process parameters such as raster angle, infill pattern and build orientation on the surface roughness and tensile strength of the PLA-ABS parts by using response surface methodology. Empirical models related to response and process parameters were developed and tested using ANOVA. Surface roughness of the parts has been measured using stylus probe surface roughness tester and tensile property has been studied using Tinius Olsen H50K2 tensile testing machine. The fracture interface has been studied using Scanning electron microscope (SEM) to understand the failure mode of the component under various loading conditions.

2 Materials and Methods

The test specimen was designed using PTC CREO Parametric 6.0 software and dimension were fixed according to the American Society for Testing and Materials (ASTM) standards, ASTM D638 type-IV for tensile testing of plastic material[9]. The width and thickness of the cross-section are 6 mm and 3.2 mm. The gauge length, overall length, and overall width

are 25 mm, 115 mm, and 19 mm as shown in Fig. 3. The specimen was exported as. STL file and imported into Idea maker 3.4.2 software to slice the model and generate G-codes for tool path deposition. All the test specimens were built using PLA-ABS material with PLA of 80% and ABS of 20% which is an amorphous thermoplastic blend as shown in Fig. 4.

PLA-ABS filament used in this research has a diameter of 0.4 mm. The three process parameters with three levels considered for experimental investigations are shown in Table 1. All the other parameters except raster angle, infill pattern and build orientation are kept constant and their respective values are shown in Table 2. The test specimens were fabricated using the FDM machine Raise 3D V2N2 with a maximum built size of 300 x 300 x 300 mm. The parts are built by depositing the semi-molten material in the form of layer with thickness of 0.3 mm. The extruder temperature and print bed temperature were set at 215°C and 110°C where these temperatures are considered to be the desired for

Table 1— Process parameters and their levels

Parameters	Levels		
	1	2	3
Raster angle (°)	0	45	90
Infill Pattern	Honeycomb	Rectilinear	Grid
Build orientation (°)	0	45	90

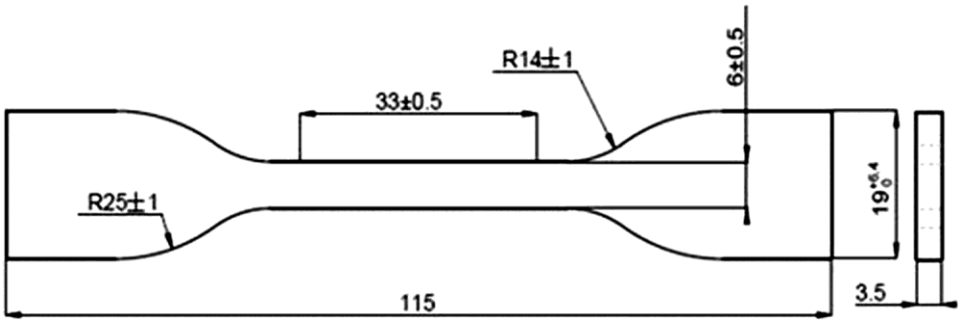

Fig. 3 — Tensile test specimen as per ASTM D638 type IV (unit: mm).

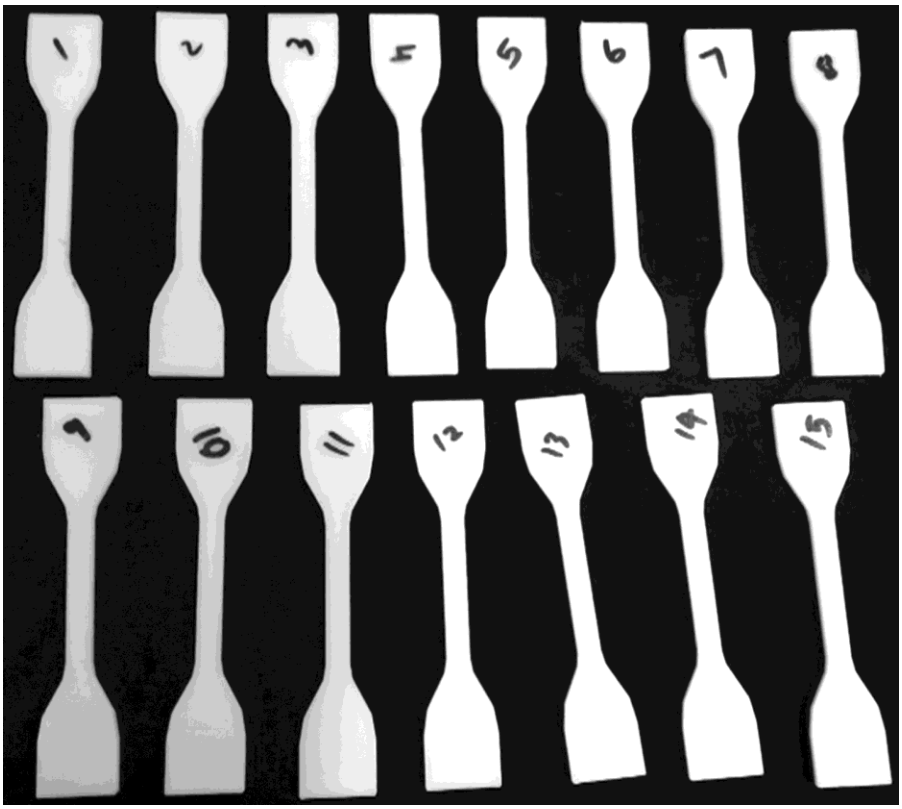

Fig. 4 — Specimens fabricated as per ASTM D638 type IV standard.

Table 2 — FDM parameters kept constant during process

Parameters	Values
Layer height	0.3 mm
Shells	2 shell
Nozzle diameter	0.4 mm
Infill	25%
Printing speed	60 mm/sec
Temperature	215°C
Outer shell speed	25 mm/sec
Inner shell speed	40 mm/sec
Infill speed	60 mm/sec
Bottom / Top layer	3 layers

the process. Three replications of each experimental trial were performed to confirm the repeatability of the results and the average value was considered for the study. The tensile test was performed using Tinius Olsen H50K2 machine. The maximum load which can be applied to this machine is 25 KN. Tensile testing of the specimens were conducted on universal tensile testing (UTM) machine at a cross-head speed of 5 mm/min as per ASTM D638 as shown in Fig. 5. Both the ends of the specimen are griped and tightened by the jigs. The crosshead motion is stopped at the moment of specimen fractures are observed. The surface roughness of the specimen was measured by a using conventional stylus probe instrument (SJ-201, Mitutoyo, Japan) with cut-off length of 0.8 mm and total measured length of 4 mm as shown in Fig. 6. Fracture behaviour of the specimens was studied by analyzing the fracture regions through SEM images[10].

Analysis of Variance (ANOVA) has been performed to statistically evaluate the effects of process parameters and their interaction on response parameters[3]. ANOVA was carried out with 95% confidence level considering all experimental trials and their responses. According to ANOVA method, R^2, S and adjusted R^2 represents coefficient of determination, standard deviation and number of predictors in the model. When R^2 and adjusted R^2 value is high, the better the model fits the data and provides the relationship between process parameters and responses. Lower the value of standard deviation (S), better the model predicts the response.

3 Results and Discussion

3.1 Ultimate tensile strength

The fabricated specimens and the corresponding ultimate tensile strength are shown in Fig. 7. The specimen fabricated with the raster angle of 0°, honeycomb infill pattern and build orientation of 45° has the highest ultimate tensile strength of 36.3 MPa as shown in Table 3.

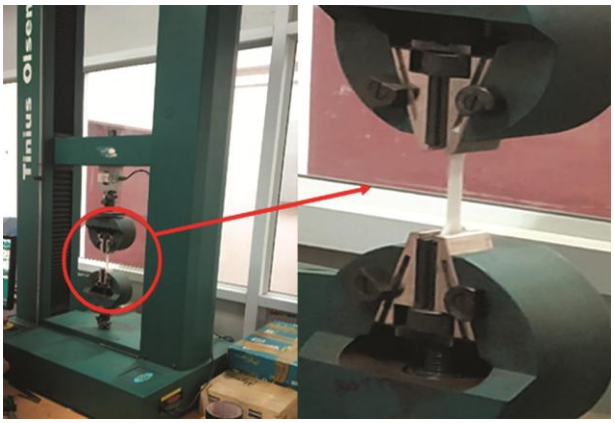

Fig. 5 — Experimental setup for tensile test.

Fig. 6 — Surface roughness measurement setup.

The second highest ultimate tensile strength of 36.2 MPa was obtained for the combination with raster angle of 90°, honeycomb infill pattern and build orientation of 45°. The specimen fabricated with honeycomb pattern exhibits high strength before failure, where the build orientation and raster angle influences the ultimate tensile strength.

The ultimate tensile strength was found to be maximum for raster angle of 0° and minimum for raster angle of 90°. Minimum value of raster angle leads to minimum distortions and strong interlayer bonding due to the alignment of layers parallel to the tensile loading conditions and thus produces high strength before failure[22,23]. When raster angle is maximum, short raster length creates voids, interlayer cracking and distortion due to residual stresses. This leads to minimum ultimate tensile strength. At 45° raster angle, specimen failed along the line of deposited layers due to brittle shear and presence of porosity causes early failure compared to 0° and 90°. Ultimate tensile strength increases when build

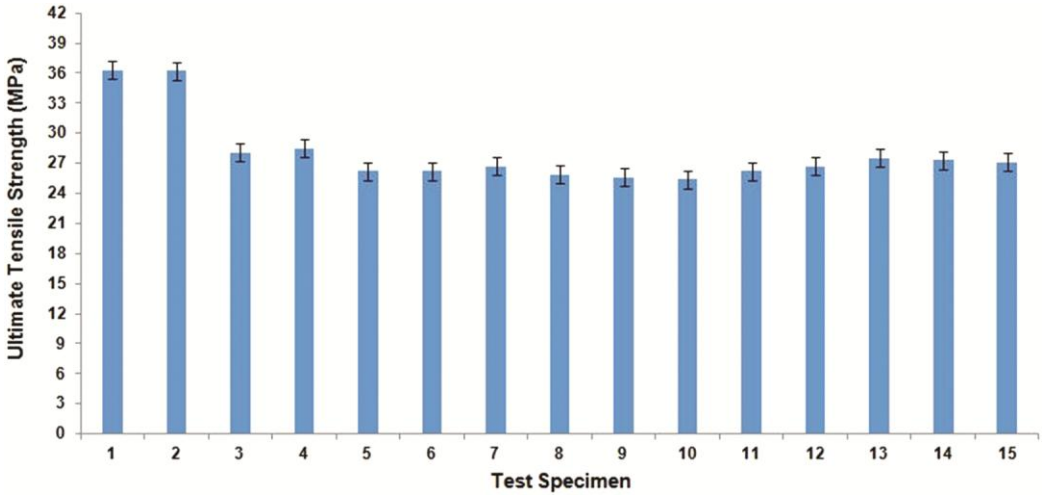

Fig. 7 — Ultimate tensile strength of fabricated specimens.

Table 3 — Results of tensile test and surface roughness

Specimens	Raster angle (degree)	Infill pattern	Build orientation (degree)	Ultimate tensile strength (MPa)	Average surface roughness R_a (μm)
1	0	Honeycomb	45	36.3	3.15
2	90	Honeycomb	45	36.2	2.71
3	0	Grid	45	28.5	3.99
4	90	Grid	45	28.1	3.09
5	0	Rectilinear	0	26.7	3.06
6	90	Rectilinear	0	26.2	2.54
7	0	Rectilinear	90	26.1	3.76
8	90	Rectilinear	90	25.9	3.49
9	45	Honeycomb	0	26.7	3.23
10	45	Grid	0	26.3	2.81
11	45	Honeycomb	90	25.6	5.72
12	45	Grid	90	25.4	2.75
13	45	Rectilinear	45	26.5	4.17
14	45	Rectilinear	45	26.3	3.50
15	45	Rectilinear	45	26.2	3.07

orientation is increased from 0° to 45° and it decreases when it is increased from 45° to 90°. When build orientation is minimum the deposited layers are parallel to the loading direction, so maximum tensile strength is observed[3,24]. When build orientation is maximum, early failure occurs due to the short orientation of raster are perpendicular to loading conditions[25]. Honeycomb pattern has high tensile strength compared to other patterns, due to the efficient hexagonal configuration. In honeycomb structure the solid layers are continuous at the fillet area to provide better rigidity. Tensile strength is minimum for grid and rectilinear patterns due to the weaker bonding exits between layers which are discontinuous in the fillet area[26].

The influences of the FDM process parameter on ultimate tensile strength were determined with ANOVA. The significance level (alpha) used in the analysis is 0.05. If P value is lesser than the alpha value of 0.05, factors are considered as significant[27]. Table 4 shows that the infill pattern, second order raster angle, second order infill pattern, second order build orientation and interaction effect of infill pattern and build orientation have significant impact on ultimate tensile strength since their P value is less than 0.05. The model is considered as statistically significantly because the P value for model is 0. The model developed using the analysis for ultimate tensile strength is shown in Eq. (1).

The experimental results were compared with the results predicted from the model obtained through ANOVA for ultimate tensile strength as shown in Table 5. The average error between the experimental and the predicted result is very less. The mathematical

Table 4 — ANOVA for ultimate tensile strength

Source	DF	Seq SS	Adj SS	Adj MS	F-Value	P-Value	Contribution
Model	9	149.772	149.772	16.6414	58.92	0.000	99.07%
Linear	3	31.018	31.018	10.3393	36.61	0.001	20.52%
Raster angle	1	0.284	0.284	0.2843	1.01	0.362	0.19%
Infill pattern	1	30.506	30.506	30.5059	108.01	0.000	20.18%
Build orientation	1	0.228	0.228	0.2278	0.81	0.410	0.15%
Square	3	111.479	111.479	37.1597	131.56	0.000	73.74%
Raster angle x Raster angle	1	24.679	23.611	23.6107	83.59	0.000	16.32%
Infill pattern x Infill pattern	1	39.511	32.927	32.9269	116.58	0.000	26.13%
Build orientation x Build orientation	1	47.289	47.289	47.2891	167.43	0.000	31.28%
2-way interaction	3	7.275	7.275	2.4250	8.59	0.020	4.81%
Raster angle x infill pattern	1	0.689	0.689	0.6889	2.44	0.179	0.46%
Raster angle x build orientation	1	0.160	0.160	0.1600	0.57	0.486	0.11%
Infill pattern x build orientation	1	6.426	6.426	6.4262	22.75	0.005	4.25%
Error	5	1.412	1.412	0.2824			0.93%
Total	14	151.184					100.00%
Standard deviation (S)	=0.531457						
R^2	=99.07 %						
R^2-adjusted	=97.38 %						
R^2-predicted	=85.78 %						

Table 5 — Comparison between experimental and predicted values of ultimate tensile strength

Test specimen	Experimental values (MPa)	Predicted values (MPa)	Error (%)
1	36.3	34.92	3.801
2	36.2	35.396	2.220
3	28.1	31.064	10.548
4	28.5	29.88	4.842
5	26.2	26.223	0.087
6	26.2	26.215	0.057
7	26.7	26.735	0.131
8	25.9	25.912	0.046
9	25.6	29.25	14.25
10	25.4	23.59	7.125
11	26.2	27.29	4.160
12	26.7	26.754	0.202
13	27.5	27.532	0.116
14	27.3	27.381	0.296
15	27.1	27.723	2.298
			Average=3.345

model error for ultimate tensile strength ranges from 0.046% to 14.25% with the mean value of 3.345. Hence, the proposed mathematical model considered as the valid model to reproduce the specimen with less deviation from predicted value of ultimate tensile strength. This shows that response parameter obtained from the experimental investigation is highly accountable and valid.

Figure 8 shows the comparison plot between experimental and predicted values of ultimate tensile strength, which indicates that the predicted values are in good agreement with experimental values. All values fall close to the trend line, this indicates that the error between the actual and predicted values is very less and the model is valid.

Ultimate tensile strength =
43.63 – 0.0937 raster angle – 14.75 infill pattern + 0.1109 build orientation + 0.001249 raster angle x raster angle + 2.986 infill pattern x infill pattern – 0.001767 build orientation x build orientation 0.00922 raster angle x infill pattern – 0.000099 raster angle x build orientation + 0.02817 infill pattern x build orientation … (1)

3.2 Surface roughness

Arithmetic average roughness (Ra) is measured at three locations and the average value is considered for study. Ra is the arithmetic average of the absolute values of the profile height deviations from the mean line and it is considered as the surface roughness parameter[10]. Surface roughness value of the fabricated specimens is shown in Fig. 9.

Minimum surface roughness value is obtained for specimen built at raster angle of 90°, rectilinear infill pattern and build orientation of 0°. Surface roughness increases when raster angle increases from 0° to 45° and decrease further increases of raster angle[2] from 45° to 90°. Increase in raster angle increases number of raster with short length, hence number of heating and cooling cycle increases to solidify the material as per the FDM fabrication principle. This cause thermal

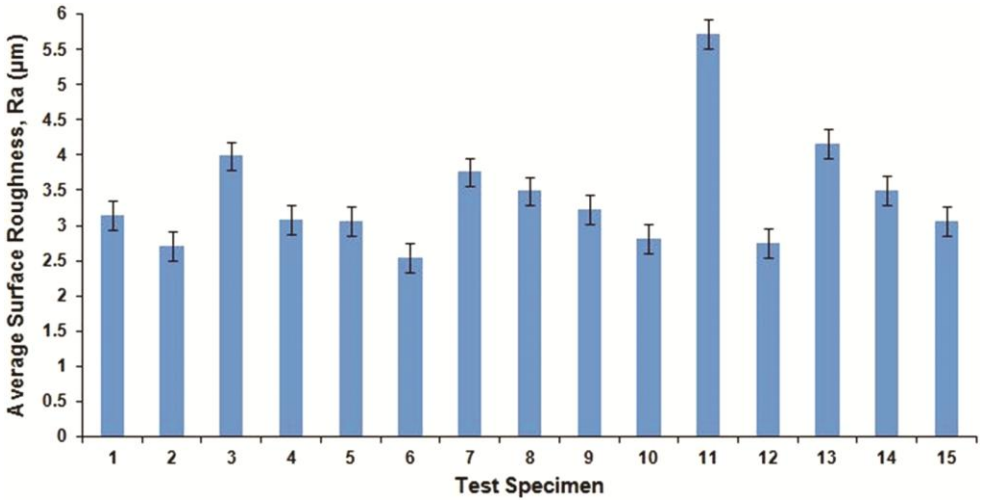

Fig. 8 — Predicted values versus the experimental values for ultimate tensile strength.

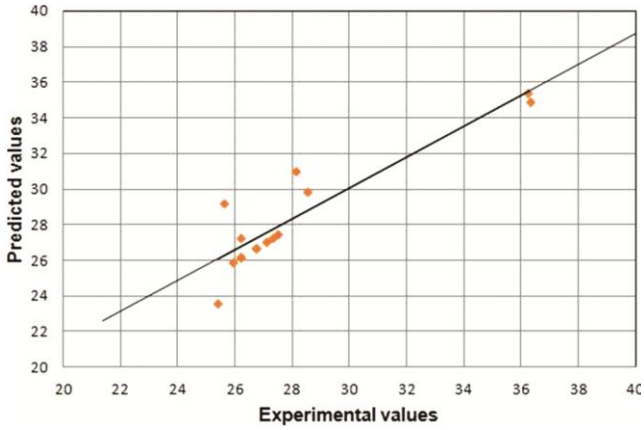

Fig. 9 — Surface roughness of fabricated specimens.

distortion which leads to poor surface finish. When raster length is shorter, fluctuation occurs at straightness of deposited road length due to adjustment of nozzle for synchronization in two directions. This fluctuation increases the surface roughness value of the specimen. Better surface finish was observed for specimens build with minimum raster angle and build orientation[2]. Minimum raster angle and build orientation reduces the non-uniform thermal stress and distortion by decreasing the heating and cooling cycles. This improves the straightness of the road width and provides better surface finish. Honeycomb pattern has high surface roughness compared to rectilinear and grid pattern due to hexagonal configuration, where the change in alignment direction results in uneven deposition and variation in material flow rate[28].

The influence of the raster angle, infill pattern and build orientation on surface roughness is determined with ANOVA. The coefficient of determination (R^2), standard deviation (S), adjusted R^2 values are obtained from ANOVA results. If P value is lesser than the alpha value of 0.05, factors are considered as significant. Table 6 shows that the raster angle, infill pattern, build orientation, second order raster angle and interaction effect of infill pattern and build orientation have significant impact on surface roughness since their P value is less than 0.05. The model is considered as statistically significantly because the P value for model is 0. The model developed using the analysis for surface roughness is shown in Eq. (2).

The experimental results were compared with the results predicted from the model obtained through ANOVA for surface roughness as shown in Table 7. The average error between the experimental and the predicted result is very less. The mathematical model error for surface roughness ranges from 0.065% to 23.985% with the mean value of 10.223. Hence, the proposed mathematical model considered as the valid model to reproduce the specimen with less deviation from predicted value of surface roughness. This shows that response parameter obtained from the experimental investigation is highly accountable and valid.

Figure 10 shows the comparison plot between experimental and predicted values of surface roughness, which indicates that the predicted values are in good agreement with experimental values. All values fall close to the trend line, this indicates that the error between the actual and predicted values is very less and the model is valid.

Surface roughness=
0.298 + 0.01381 raster angle +
0.307 infill pattern +

Table 6 — ANOVA for surface roughness

Source	DF	Seq SS	Adj, SS	Adj MS	F-Value	P-Value	Contribution
Model	9	3.67833	3.67833	0.40870	40.52	0.000	98.65%
Linear	3	1.86516	1.86516	0.62172	61.64	0.000	50.02%
Raster angle	1	0.22950	0.22950	0.22950	22.75	0.005	6.15%
Infill pattern	1	0.48956	0.48956	0.48956	48.53	0.001	13.13%
Build orientation	1	1.14610	1.14610	1.14610	113.62	0.000	30.74%
Square	3	0.34822	0.34822	0.11607	11.51	0.011	9.34%
Raster angle x Raster angle	1	0.33189	0.31339	0.31339	31.07	0.003	8.90%
Infill pattern x Infill pattern	1	0.00437	0.00552	0.00552	0.55	0.493	0.12%
Build orientation x Build orientation	1	0.01196	0.01196	0.01196	1.19	0.326	0.32%
2-way interaction	3	1.46495	1.46495	0.48832	48.41	0.000	39.29%
Raster angle x Infill pattern	1	0.05290	0.05290	0.05290	5.24	0.071	1.42%
Raster angle x Build orientation	1	0.00189	0.00189	0.00189	0.19	0.683	0.05%
Infill pattern x Build orientation	1	1.41016	1.41016	1.41016	139.80	0.000	37.82%
Error	5	0.05043	0.05043	0.01009			1.35%
Total	14	3.72876					100.00%
Standard deviation (S)	=0.100432						
R^2	=98.65%						
R^2-adjusted	=96.21%						
R^2-predicted	=85.60%						

Table 7 — Comparison between experimental and predicted values of surface roughness

Test specimen	Experimental values (μm)	Predicted values (μm)	Error (%)
1	3.15	3.489	10.761
2	2.71	3.355	23.800
3	3.99	3.345	16.165
4	3.09	2.751	10.970
5	3.06	3.062	0.065
6	2.54	2.703	6.417
7	3.76	3.764	0.106
8	3.49	3.498	0.229
9	3.23	2.912	9.845
10	2.81	3.484	23.985
11	5.72	4.872	14.825
12	2.75	3.067	11.527
13	4.17	3.581	14.124
14	3.5	3.512	0.342
15	3.07	3.383	10.195
			Average=10.223

0.03179 build orientation –
0.000144 raster angle x raster angle +
0.0387 infill pattern x infill pattern +
0.000028 build orientation x build orientation –
0.00256 raster angle x infill pattern +
0.000011 raster angle x build orientation –
0.01319 infill pattern x build orientation

…(2)

3.3 Fracture analysis

Scanning Electron Microscope (SEM) images was used to study fracture surface of the specimen after tensile testing. The failure occurred due to the material separation in a direction perpendicular to tensile loading conditions. The brittle failure mechanism was observed at perpendicular direction to tensile loading for specimen build with raster angle of 0°. The presence of voids and interlayer porosity in specimen reduce the tensile strength and leads to early failure as shown in Fig. 11. The specimen build at raster angle of 45° failed due to brittle shear mechanism, where each raster are pulled out during tensile loading condition. The specimen build at 90° raster angle failed due to thermal distortion and weak bonding between adjacent layers[2,29]. Brittle fracture was observed for specimen build with 0° and 45° orientation and inter-raster failure occurs for 90° build

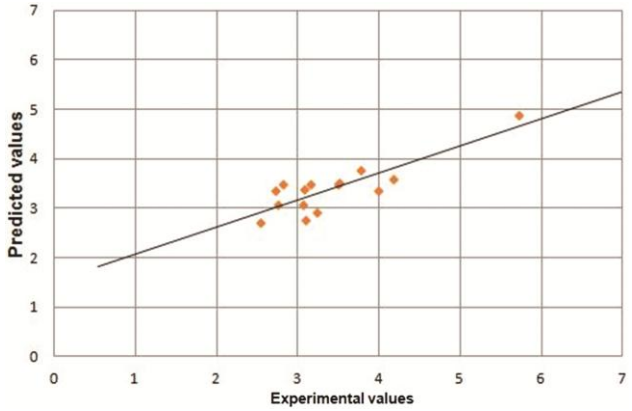

Fig. 10 — Predicted values versus the experimental values for surface roughness.

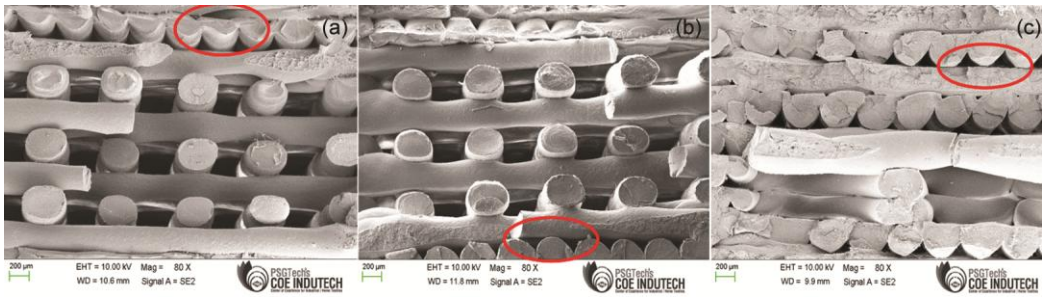

Fig. 11 — SEM images of the fracture surface of the specimens (a) 0^o, (b) 45^o, and (c) 90^o raster angle.

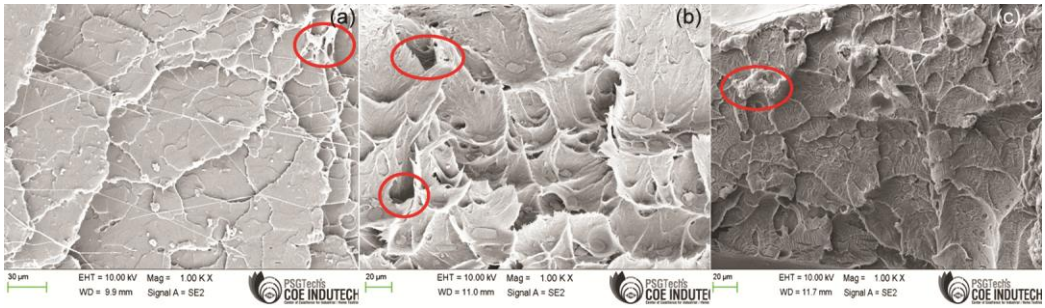

Fig. 12 — SEM images of the fracture surface of the specimens (a) 0^o, (b) 45^o, and (c) 90^o build orientation.

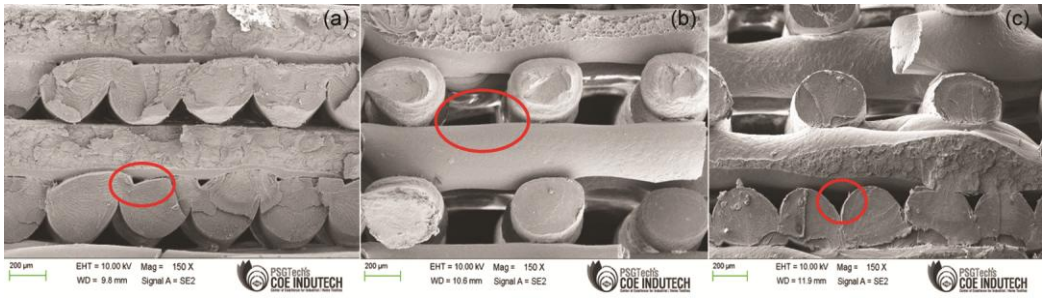

Fig. 13 — SEM images of the fracture surface of the specimens (a) honeycomb, (b) grid, and (c) rectilinear infill pattern.

orientation due to presence of weak interlayer bond and thermal stresses as shown in Fig. 12. Grid infill pattern shows brittle fracture and rectilinear infill pattern shows partial brittle-ductile fracture mechanism because raster are pulled out to the direction perpendicular to tensile loading conditions. In honeycomb pattern, inter-raster failure was observed because changes in alignment of raster make short raster length which generates minor gaps between adjacent raster as shown in Fig. 13. Trans-raster failure was observed on the components built with long edge orientation. During the process, more heat is available at the bottom of the components so it is closely packed and minor gaps are observed at the mid section of the components due to insufficient time to coalesce completely before solidification which leads to failure.

4 Conclusion

In this work, an experimental investigation has been carried out to study the influence of raster angle, infill pattern and build orientation on the ultimate tensile strength and surface roughness of FDM manufactured specimens using PLA material. Statistical analysis has been carried out using ANOVA to identify the influence of process parameters.

Higher ultimate tensile strength has been obtained for the specimen built at raster angle of 0°, honeycomb infill pattern and build orientation of 45°. ANOVA result has showed that infill pattern was the most significant process parameter for tensile strength, followed by the build orientation and raster angle. The interaction effect of infill pattern and build orientation was also found to be significant factor for tensile strength.

Minimum surface roughness value obtained for the specimen built with raster angle of 90°, rectilinear infill pattern and build orientation of 0°. ANOVA result has showed that build orientation was the most significant process parameter for surface roughness,

followed by the infill pattern and raster angle. The interaction effect of infill pattern and build orientation was also found to be significant for surface roughness.

Fractography study indicated that part built with grid infill pattern failed under brittle mode and part built with rectilinear infill pattern showed partial brittle-ductile fracture failure mechanism. Inter-raster failure mode has been observed in part built with honeycomb pattern.

References

1 Abdelrhman A M, Gan W W, & Kurniawan D, *IOP Conference Series: Materials Science and Engineering*, 694 (2019) 012048.
2 Keles O, Blevins C W, & Bowman K J, *Rapid Prototyp J*, 23 (2017) 320.
3 Dave H K, Patadiya N H, Prajapati A R, & Rajpurohit S R, *Proc Inst Mech Eng-PartC J Mech Eng Sci*, 235 (2021) 1.
4 Leite M, Varanda A, Ribeiro A R, Silva A, & Vaz M F, *Rapid Prototyp J*, 24 (2018) 195.
5 Wang L, Sanders J E, Gardner D J, & Han Y, *Prog Addit Manuf*, 3 (2018) 205.
6 Onwubolu G C, & Rayegani F, *Int J Manuf*, 1 (2014) 13.
7 Mohamed O A, Masood S H, & Bhowmik J L, *Measurement*, 107 (2017) 128.
8 Garg A, Bhattacharya A, & Batish A, *Proc Inst Mech Eng-PartB J Eng Manuf*, 231 (2017) 2031.
9 Liu X, Zhang M, Li S, Si L, Peng J, & Hu Y, *Int J Adv Manuf Tech*, 89 (2017) 2387.
10 Park S L, Hong G W, Kim J, & Kim J H, *J Mech Sci Technol*, 33 (2019) 5235.
11 Samykano M, Selvamani S K, Kadirgama K, Ngui W K, Kanagaraj G, & Sudhakar K, *Int J Adv Manuf Tech*, 102 (2019) 2779.
12 Srivastava M, Maheswari S, Kundran T K, Yashaswi R, & Rathee S, *CAD/CAM, Robotics and Factories of the Future* (Springer, India), 1st Edn, ISBN:9788132227403, 2016, p.301.
13 Zaman U K U, Boesch E, Siadat A, Rivette M, & Baqai A A, *Int J Adv Manuf Tech*, 101 (2019) 1215.
14 Kuo C C, Wu Y R, Li M H, & Wu H W, *Int J Adv Manuf Tech*, 101 (2019) 593.
15 Kelkar A S, Kumbhar N N, & Mulay A V, *J Inst Eng India Ser C*, 99 (2018) 429.
16 Jo K H, Jeong Y S, Lee J H, & Lee S H, *Int J Precis Eng Manuf*, 17 (2016) 1541.
17 Jin Y, Wan Y, Zhang B, & Liu Z, *J Mater Process Technol*, 240 (2017) 233.
18 Ang K C, Leong K F, & Chua C K & Chandrasekaran M, *Rapid Prototyp J*, 12 (2006) 100.
19 Dawoud M, Taha I, & Ebeid S J, *J Manuf Process*, 21 (2016) 39.
20 Ning F, Cong W, Qiu J, Wei J, & Wang S, *Compos B Eng*, 80 (2015) 369.
21 Peng A, Xiao X, & Yue R, *Int J Adv Manuf Technol*, 73 (2014) 87.
22 Zhang X, Chen L, Mulholland T, & Osswald TA, *Polym Adv Technol*, 30 (2019) 2122.
23 Afrose M F, Masood S H, Iovenitti P, Nikzad M, & Sbarski I, *Prog Addit Manuf*, 1 (2016) 21.
24 Kamaal M, Anas M, Rastogi H, Bhardwaj N, & Rahaman A, *Prog Addit Manuf*, 1 (2020) 20.
25 Uddin M S, Sidek M F R, Faizal M A, Ghomashchi R, & Pramanik A, *J Manuf Sci Eng*, 139 (2017) 1.
26 Fernandez-Vicente M, Calle W, Ferrandiz S, & Conejero A, *3D Print Addit Manuf*, 3 (2016) 183.
27 Balderrama-Armendariz C O, MacDonald E, Espalin D, Cortes-Saenz D, Wicker R, & Macias A M, *Int J Adv Manuf Tech*, 96 (2018) 307.
28 Perez M, Medina-Sánchez G, Garcia-Collado A, Gupta M, & Carou D, *Materials*, 11 (2018) 1382.
29 Wang L, & Gardner D J, *Prog Addit Manuf*, 3 (2018) 165.